Local Ocean-Atmosphere Interaction in Indian Summer Monsoon Multi-Decadal Variability

Dhruba Jyoti Goswami
University of Hyderabad
Ashok Karumuri
University of Hyderabad
Bhupendranath Goswami (bhupengoswami100@gmail.com)
Cotton University

Research Article

Keywords: Multi-decadal mode, tropical Indian Ocean, Bjerknes feedback, large-scale vorticity feedback, net heat flux

Posted Date: December 22nd, 2021

DOI: https://doi.org/10.21203/rs.3.rs-788323/v2

Abstract

The significant multi-decadal mode (MDM) of the Indian summer monsoon rainfall (ISMR) during the past two millennia provides a basis for decadal predictability of the ISMR and has a strong association with the North-Atlantic variability with the Atlantic Multi-decadal Oscillation (AMO) as a potential external driver. It is also known that the annual cycles and interannual variability of ISMR and sea surface temperatures (SST) over the tropical Indian Ocean (IO) are strongly coupled. However, the role of local air-sea interactions in maintaining or modifying the ISMR MDM remains unknown. A related puzzle we identify is that the IO SST has an increasing trend during two opposite phases of the ISMR MDM, namely during an increasing phase of ISMR (1901 to 1957) as well as a decreasing phase of ISMR (1958-2007). Here, using a twentieth-century reanalysis (20CR), we examine the role of air-sea interactions in maintaining two opposite phases of the ISMR MDM and unravel that the Bjerknes feedback is at the heart of maintaining the ISMR MDM but cannot explain the increasing trend of SST in the tropical IO during the opposite phases. Large-scale low-level vorticity influence on SST and net heat flux changes through circulation and cloudiness changes associated with the two phases of the ISMR MDM together contribute to the SST trends. The decreasing trend of low-level wind convergence during the period between 1958 and 2007 is a determining factor for the decreasing trend of ISMR in the backdrop of an increasing trend of atmospheric moisture content. Consistent with the lead of the AMO with respect to ISMR by about a decade, the AMO drives the transition from one phase of ISMR MDM to another by changing its phase first and setting up low-level equatorial zonal winds conducive for the transition.

Introduction

The share of agriculture in the gross domestic product (GDP) of India hovered between 17 and 19 percent during 2003 and 2020 and reached almost 20 percent making it a bright spot in the GDP performance of the country during 2020-21, according to the Economic Survey 2020-2021 (Kapil 2021). Dependence of the country's economy on agriculture makes the socio-economic welfare of the large population of the region vulnerable to the vagaries of the ISMR with both the total food production as well as the GDP strongly correlating with the ISMR (Webster et al. 1998; Parthasarathy et al. 1988; Gadgil and Gadgil 2006; Amat et al. 2018, 2021). The seasonal rainfall anomalies during extremes of ISMR year-to-year variability manifesting in the large scale 'floods' and 'droughts' tend to be homogeneous over the country (Shukla 1987) as also evident from the dominant pattern of the year-to-year variability of the ISMR (Mishra et al. 2012; Choudhury et al. 2021). Therefore, a forewarning of even the quantum of seasonal rainfall over the country (ISMR) one season in advance is useful for the policymakers and farmers and has a long history in India starting with Blanford (1884) and Walker (1924). For the same reason, longer lead forecasts of ISMR such as at 6-month or 12-month leads would be highly useful for farmers and policymakers to plan for water resources and for alternative crop strategies to minimize loss. However, even the one season forecast of ISMR has remained a grand challenge problem (Goswami and Krishnan 2013) and almost no attempt has been made for a longer lead forecast of ISMR. Only recently, statistically significant but still moderate skills are being achieved (Rao et al. BAMS 2019).

Potentially the ISMR, as a measure of the Indian summer monsoon, is a highly predictable system (Charney and Shukla 1981, Saha et al. 2019) and the predictability comes from association of the ISMR with some predictable slowly varying drivers such as the El Niño and Southern Oscillation (ENSO) and the Atlantic Multi-decadal Oscillation (AMO). One of the challenges in seasonal prediction of ISMR has been that the interannual correlation between ISMR and the predictors undergo significant epochal variations (Kripalani and Kulkarni 1997; Krishnamurthy and Goswami 2000; Kumar et al. 1999; Xavier et al. 2007). This epochal variability is partly due to the inherent significant multi-decadal variability of ISMR (Kriplani and Kulkarni 1997; Goswami et al. 2006a; Goswami et al. 2015) and the predictors like the ENSO (Zhang et al. 1997), the AMO, and the Pacific Decadal Oscillations (PDO, Mantua and Hare 2002). A model decomposition of long time series of instrumental records of ISMR (1813-2006, Sontakke et al. 2008) indicates that apart from a quasi-biennial mode (2.7-year period), the MDM with period around 65-years is the only other statistically significant mode of ISMR variability (Rajesh and Goswami 2020). That the MDM of ISMR with a period of around 65-years is a robust mode of ISMR variability is evident in rainfall reconstruction from tree ring records for more than 500 years in south India (Goswami et al. 2015) and in oxygen isotope records (correlated with rainfall amount) in cave deposits from central India/north India over the past two millennia (Sinha et al. 2011, 2015). The MDM of ISMR influences or modulates the seasonal predictability through modulation of its interannual variability. From the instrumental record of ISMR, it has been observed that the frequency of occurrence of floods (droughts) increases (decreases) by a factor of 2 during the positive (negative) phases of ISMR MDM (Rajesh and Goswami 2020). The inability to simulate the AMO and ISMR MDM with fidelity by climate models has one roadblock to improving skill of seasonal predictions systems of today. The CMIP6 models are showing notable improvement in simulating the AMO as well as ISMR MDM (Choudhury et. al., 2021) with optimism for improving ISMR prediction in coming years. A better understanding of the drivers of the MDM of ISMR and associated teleconnection mechanisms is, therefore, critical for simulating the same by climate models and making advances in seasonal prediction of ISMR.

Its robust existence during the past two millennia indicates that the MDM of ISMR with an approximate period of around 65 years is a natural mode of the South Asian monsoon system. What drives the MDM of ISMR has been the subject of intense investigation in recent years. On centennial and millennial time scales, paleo-evidences indicate strong linkages between mega-droughts of Indian monsoon and cooling of North Atlantic water (Burns et al. 2003; Gupta et al. 2003). Analysis of instrumental records of ISMR and SST over the North Atlantic reveal a significant association between the two on multi-decadal time scales as well (Goswami et al. 2006a) and the teleconnection is supported by coupled model simulations (Zhang and Delworth 2006; Wang et al. 2009; Luo et al. 2011, 2018). In a recent study, Borah et al. (2020) show that all the non-El Niño droughts of ISMR are associated with cooling of the North Atlantic associated with the negative phases of the AMO. The potential for the AMO to enhance the predictability of ISMR led to explore the teleconnection mechanisms between the AMO and the seasonal mean ISMR in several recent studies. Goswami et al. (2006a) proposed that the North Atlantic SST associated with the AMO sets up a stationary wave and influences the ISMR through modulating the tropospheric temperature gradient (TTG) over the Indian monsoon region, a mechanism that was supported by a

number of modeling studies (Lu et al. 2006; Li et al. 2008). The nature of the stationary wave has been elucidated in the form of a Rossby wave train in some recent studies (Syed et al. 2012; Krishnamurthy and Krishnamurthy 2016; Borah et al. 2020; Rajesh and Goswami 2020). As the seasonal mean ISMR is intimately linked to the statistics of sub-seasonal fluctuations such as frequency of occurrences, variances etc. (Palmar 1994; Goswami et al. 2006b; Saha et al. 2019), how the stationary Rossby wave train associated with the AMO influences the ISMR through sub-seasonal evolution, however, remains unclear. For the case of non-El Niño ISMR droughts, Borah et al. (2020) showed that the modulation of the large scale circulation by the Rossby wave train clusters the monsoon 'breaks' in one phase of the seasonal cycle leading to a 'long break' and resulting in weakening of the ISMR. Generalizing the Borah et al. (2020) study, Rajesh and Goswami (2020) show that during the positive (negative) phase of the AMO, similar Rossby wave trains cluster 'active' ('break') phases in one segment of the seasonal cycle leading to 'long active' ('long break') spells and resulting in strengthening (weakening) of the seasonal mean ISMR. While the teleconnection is largely through an atmospheric bridge, the possibility of an oceanic bridge involving the Atlantic Meridional Overturning Circulation (AMOC) is also indicated (Rajesh and Goswami 2020) while a detailed pathway remains unknown. The Rossby wave train appears to be set up by episodic barotropic vorticity forcing over the SST anomalies in the North-Atlantic (Borah et al. 2020). Unlike in the tropics, the extra-tropical SST being largely a response of atmospheric forcing, the driving of the episodic barotropic vorticity remained unclear. While on high frequency synoptic time scale, indeed the atmospheric fluxes determine the SST, on time scales longer than 10-days, large scale SST anomalies could influence meridional surface pressure gradients, displace the storm tracks and create stationary barotropic vorticity (Rajesh and Goswami 2020; Goswami et al. 2021). Thus, compelling evidence has emerged for AMO as a major driver of the ISMR MDM. An alternative pathway to the modulation of the sub-seasonal oscillations by the Rossby wave train has been indicated in some recent studies (Sun et al. 2017, 2018) where it is shown that the AMO could influence ISMR on decadal to multi-decadal time scale through modulation of western Pacific SST, which in turn influence the Arabian Sea SST through a regional atmospheric bridge thereby influencing the moisture flux to the Indian monsoon region.

The Indian summer monsoon system, on the other hand, is a coupled ocean atmosphere system where local ocean-atmosphere interactions not only maintain the annual cycle of SST in the region, the Inter-Tropical Convergence Zone (ITCZ) and monsoon rainfall (Webster et al. 1998; Wang et al. 2005) but also actively influence intra-seasonal (Sengupta and Ravichandran 2001; Kembell-Cook and Wang 2001; Lau, Waliser and Goswami 2012 for a review) and interannual variability of ISMR (Loschnigg and Webster 1999; Meehl and Arblaster 2002; Meehl 1994). The Indian Ocean Dipole Mode (Saji et al. 1999; Webster et al. 1999; Ashok et al. 2001) is another example of local ocean-atmosphere interactions leading to interannual variability of climate in the region. While the driving of the ISMR MDM by the AMO through teleconnections is emerging, the roles of local air-sea interactions or other external forcing (e. g. anthropogenic aerosols) are unknown. Studies such as Ashok et al. (2004) and Marathe et al. (2021) have also suggested slower decadal variability in the tropical Indian Ocean modes, at least in the model world. Ashok et al. (2004), for example, suggest that the decadal variability of the monsoons leads to decadal IOD-like variability. The decreasing trend of ISMR between 1951 and 2000 has received attention

and has been the subject matter of several studies lately. Through a modeling study, Bollasina et al. (2011) indicate that the cooling due to anthropogenic aerosols is responsible for the decreasing trend of ISMR during the period. The revival of the ISMR after 2002, however, is not consistent with aerosol as primary forcing (Jin et al. 2017). In another interesting study, Swapna et al. (2014) show that the increasing trend of SST over the IO is responsible for the decreasing trend of ISMR during this period (1951-2007) while the weakening trend of ISMR support the increasing trend of SST, through circulation and flux changes, indicating positive feedback. Again, the revival of the ISMR after 2002 (Jin et al. 2017) while the SST is still increasing is also inconsistent solely with positive feedback. Here, we explore a hypothesis that the ISMR MDM is largely driven by teleconnection with the AMO through modulation of the regional circulation but the observed periodicity and amplitude of the ISMR MDM is a result of modification through local air-sea interactions and aerosol forcing.

Our hypothesis is rooted in the following observations. A longer time series of ISMR (Fig. 1) shows that while there is a decreasing trend of ISMR during 1951-2000, it has an increasing trend during 1901-1950 in the backdrop of an increasing trend of SST during the entire period. The two epochs are approximately two opposite phases of the ISMR MDM. Therefore, it is clear that the selective focus on the decreasing trend of ISMR during 1951 and 2007 could be misleading as the increasing trend of ISMR during the period between 1901 and 1950 is associated with an increasing trend of SST over the IO. As an extension of Swapna et al. (2014), we ask, what type of ocean-atmosphere interaction is operative in the increasing phase of the ISMR MDM? Here, we investigate the nature of air-sea interaction during two contrasting phases of ISMR multi-decadal variability, namely period P1 (1901-1957) when the ISMR has an increasing trend and period P2 (1958-2007) when the ISMR has a decreasing trend. The insight gained from this exercise indicates that the air-sea interaction is a stable air-sea interaction where another positive feedback is triggered by non-local modulation of circulation through teleconnections.

Data And Methods

2.1 Data:

In order to explore ocean-atmosphere interaction over the IO and Indian monsoon region and its relationship with ISMR, we extract several ocean variables such as sea surface height, surface current from the Simple Ocean Data Assimilation version 2 (SODA-2, Giese et al. 2011), the latest 20^{th} Century Ocean reanalysis of the SODA data releases for our study period (1901-2007). Upper layer heat content (HC) is defined as integrated heat over the upper 300 meters of the tropical IO between 20^{O}S-30^{O}N and 40^{O}E-110^{O}E. To calculate the heat content, we extract temperature and salinity data with depth from SODA-2. The sea surface temperature (SST) data is extracted from Hadley Centre Global Sea Ice and Sea Surface Temperature (HadISST, Rayner 2003). For surface winds, we had a choice of using winds from ERA-20CM (Hersbach et al. 2015) or NCEP 20^{th} century reanalysis version 3 (NCEPv3, Slivinski et al. 2019). As the surface winds in the region are coupled with the ISMR, the biases in ISMR from ERA-20CM or NCEPv3 are closely linked with the biases in the winds in the respective reanalysis. In order to gain insight into ocean-atmosphere interactions associated with the multi-decadal component of ISMR, the

reanalyzed winds used need to be consistent with similar multi-decadal variability of reanalyzed ISMR. The reanalyzed ISMR between 1901 and 2007 from NCEPv3 (Fig. 1c) and ERA-20CM (Fig. S3) indicate that the simulated NCEPv3 ISMR multi-decadal variability replicates variability of observed ISMR (Fig. 1a) reasonably well. However, the phases of simulated multi-decadal variability of ERA-20CM ISMR during 1901-1957 and 1958-2007 are opposite to that of observed ISMR. Therefore, we use the NCEPv3 winds in this study instead of ERA-20CM winds. The seasonal mean net heat fluxes (Q_{net}) are extracted from the two reanalyses (NCEPv3, ERA-20CM), calculated from net downward shortwave radiation flux, net upward longwave radiation flux, sensible heat flux, and latent. TropFlux is a hybrid product (Kumar et al. 2012) where shortwave radiation fluxes are used from International Satellite Cloud Climatology Project (ISCCP) and uses bias and amplitude corrected ERA-I (10-m winds, 2-m air, and sea temperature, 2-m air relative humidity, and downward radiative fluxes. In order to get an idea of the biases in the Q_{net} from reanalysis, we compare the climatology of the Q_{net} from reanalyses with that extracted from the TropFlux data set. To see integrated moisture convergence and water vapour, we use specific humidity data from NCEPv3. Daily gridded rainfall data (Rajeevan et al. 2006) with a resolution of 1°× 1° over the land region of India for the period 1901–2004 are used in this study.

Unless mentioned otherwise, all the datasets and the major part of the analysis pertain to the 1901-2007 period, considering the common availability period.

2.2 Methods:

2.2.1 The EOF analysis and the two feedbacks:

The Bjerknes feedback originally proposed by Bjerknes (1969) for explaining the El Nino and Southern Oscillation (ENSO) in the Pacific is applicable for the tropical Indian Ocean as well. The equatorial surface winds driven by east-west surface pressure gradients lead to thermocline adjustment via equatorial Ekman divergence (convergence) and modify the original equatorial SST gradients. Associated modification of surface pressure gradients modifies the original equatorial winds. Over the Indian Ocean during northern summer, the Bjerknes feedback is closely linked with the Indian monsoon as the monsoon heat source influences the equatorial winds in the region. As the zonal wind forcing at the equator plays a critical role in the Bjerknes feedback an empirical orthogonal function (EOF) analysis of zonal mean surface zonal winds averaged between 70°E to 90°E is carried out between 35°S and 35°N for the period 1901-1957 (P1). The dominant mode (EOF1) explains 38.9% while the EOF2 explains 25.8% of interannual variance. The dominant EOF not only explains largest interannual variance, the first principal component (PC1) is significantly correlated with ISMR (r = 0.28, p=0.03) while the PC2 has insignificant correlation with the ISMR (r =0.05,). For the period 1958-2007 (P2), EOF1 of zonal mean surface zonal winds explains 49.3% while the EOF2 explains 31.1% interannual variance. During the period P2 also, the PC1 has statistically significant positive correlation with ISMR (r =0.36, p=0.001) while the PC2 has insignificant correlation with ISMR. Therefore, we use the dominant EOF of the zonal mean surface zonal winds and the PC1 to examine the Bjerknes feedback during the two opposite phases of the ISMR multi-decadal variability.

The southeasterly cross-equatorial flow and southwesterly flow to the north of the equator as a result of the Indian monsoon heat source creates a large-scale anticyclonic vorticity around the equator. Year-to-year variation in the intensity and location of the monsoon heat source would give rise to anomalous cyclonic or anti-cyclonic large-scale vorticity around the equator. Anomalous upwelling and down welling forced by the vorticity could influence the SST over the tropical belt. Change in SST over the tropical belt leads to change in moisture flux transported and converged over the monsoon region and affect the monsoon that caused the vorticity anomaly over the equator. In order to examine this aspect of ocean atmosphere interaction, an EOF analysis carried out on the meridional shear of zonally averaged (u wind from NCEPv3) surface wind and –d[u]/dy (vorticity) over 70°E to 90°E and 35°S to 35°N during JJAS summer monsoon season for the period P1 as well as for the period P2. The first empirical mode of –d[u]/dy explains 37.33% and 43.47% of interannual variance for the periods P1 and P2 respectively. Similar to the case of first principal component of the dominant EOF of the zonal mean surface zonal wind, the PC1 of dominant EOF of the –d[u]/dy also correlate significantly with ISMR (r =0.28, p =0.03) for the period P1 but for the second period P2 the correlation between PC1 and ISMR is not significant (r =0.093, p=0.52)

2.2.2 Regression analysis:

Regression is a useful statistical tool used to determine relationships between two or more dependent and independent variables. Among all the different regression models we used linear regression in our study. A linear regression analysis has been done to find how the SST and ISMR is varying with the zonally averaged (u wind from NCEPv3) surface wind and –d[u]/dy for both the periods P1 and P2.

Results

3.1 Bjerknes Feedback

Bjerknes feedback where surface wind forcing leads to east-west SST gradient in the equatorial Pacific basin, which in turn feeds back to strengthen the original surface winds is at the heart of the ENSO (Bjerknes 1969) phenomenon. The Bjerknes feedback has been shown to be also operative in the IO, leading to the Indian Ocean Dipole mode (Saji et al. 1999; Webster et al. 1999; Murtugudde et al. 2000) on an interannual time scale. Here, we explore if a similar feedback contributes to the multi-decadal variability of the ISMR.

The modification of the SST, sea-level and HC distribution by surface winds through equatorial dynamics of Wyrtki jets (Wyrtki 1973) is an important component of ocean-atmosphere interaction in this region. For the period 1901-1957 (referred to as P1), the first empirical mode of zonally averaged surface winds explains 38.9% variance while the same for the period 1958-2007 (referred to as P2) explains 49.3% variance. The leading EOF (henceforth, referred to as EOF1) of surface winds zonally averaged over 70°E to 90°E during the two periods P1and P2 (Fig. 2a and Fig. 2b) show some interesting differences in large scale circulation during the two periods. While the deep equatorial belt was dominated by higher frequency of occurrence of easterly forcing during the early period (1901-1957), the later period is

dominated by higher frequency of occurrence of westerly wind forcing (Fig. S1b,c). The corresponding PCs (Fig. 2c,d), while having large interannual variation, do not indicate any significant trend. The propensity of zonal mean easterly wind forcing at the equator during the period P1, and westerly forcing in the period P2 contribute to the easterly trends of surface winds at the equator in the period P1 between 70□E and 100□E (Fig. 3a) as against westerly trends of surface winds at the equator during the period P2 (Fig. 3b) between 60^{o}E and 90^{o}E. The trends in the zonal winds are also consistent with trends of SST during both periods (Fig. 3a,b). Much stronger and wide-spread increasing trends of SST during P2 compared to that during P1 are consistent with a weaker increasing trend of area averaged SST in Fig. 1b compared to a relatively stronger increasing trend of area averaged SST during the period (P2) . Also, maximum SST trend during P2 is over the west-central equatorial IO, as noted in earlier studies (Swapna et al. 2014; Koll et al. 2014).

A regression of PC1 of zonally averaged zonal winds on seasonal mean rainfall anomaly over India during the periods P1 and P2 (Fig. 4a,b) show that the zonal wind variations during P1 are associated with the increasing tendency of rainfall over the core monsoon region and west of the Western Ghat consistent with Fig. 1a, while that during period P2 are associated with a decreasing tendency of rainfall over core monsoon and west of Western Ghat, consistent with Fig. 1a. The SST anomaly patterns associated with the zonal wind variations (regression with PC1) during the period P1 (P2) (Fig. 4c,d) are closely similar to a positive (negative) IOD pattern (Saji et al., 1999). They are consistent with easterly (westerly) driving as evident from Fig. S1a (Fig. S1a). During an easterly driving regime, shoaling of thermocline to the east gives rise to cold anomaly while depression of thermocline to the west gives rise to warm anomaly. The situation reverses during the westerly driving regime. During P1 the SST dipole has a cold anomaly over a smaller region in the east and a much larger region of warm anomaly to the west. In contrast, during the period P2, the SST dipole has a warm anomaly over a smaller region in the east, with a much larger region of cold anomaly to the west (Fig. 4c,d). The overall easterly (westerly) driving during P1 (P2) is due to the fact that the equatorial zonal winds averaged over (70□E to 90□E, 5□S to 5□N) have higher propensity of easterly zonal wind during P1, while the propensity of westerly zonal wind is higher during P2 (Fig. S1d,e). The easterly (westerly) winds at the equator during P1 (P2) is a result of the stronger (weaker) than normal ISMR while the warmer (colder) SST to the western part of IO as a result of equatorial dynamics leads to higher (lower) moisture flux to the continent and tends to strengthen (weaken) the monsoon further. This is how the Bjerknes feedback at the equator and ISMR, an off-equatorial heat source are linked. The decadal variability of the IOD has also been documented (e.g., Ashok et al. 2001, 2004).

We find westward surface currents around the equatorial belt, forced by predominantly easterly surface winds during the period P1 (Fig. 5a). Associated equatorial upwelling and coastal upwelling depletes the HC in the eastern IO flanked by a horseshoe pattern build-up of HC in the western IO (Fig. 5a). The off-equatorial heat depletion in the eastern IO seems to be due to episodes of equatorial upwelling Kelvin waves that were driven by the easterly winds, and subsequently travelled as a coastal Kelvin wave towards north after hitting the eastern boundary and radiated westwards as Rossby waves. The signature

of a coastal Kelvin wave in the Bay of Bengal is rather apparent (Fig. 5a). Similarly, the buildup of HC in the eastern IO during the period P2 seems to be due to episodes of down welling equatorial Kelvin waves driven by the westerly zonal winds, which subsequently have travelled north and south as coastal Kelvin waves and radiated as down welling as Rossby waves (Fig. 5b). Even in this case, coastal Kelvin waves in the Bay of Bengal could be seen clearly. The surface currents during the period P2 are also consistent with surface wind forcing. However, the westward surface currents in this case are limited to the central and eastern equatorial IO east of 70^{O}E (Fig. 5b). This explanation is supported by the sea surface height (SSH) anomaly patterns associated with zonal mean zonal winds (regression with PC1) over the two periods (Fig. 5c,d).

3.2 Large-scale vorticity of surface zonal winds and SST

While there is considerable evidence that a Bjerknes feedback operates in maintaining the MDM of ISMR, the large increasing trend of SST during the later period (P2) cannot be explained by this feedback. In fact, purely due to this feedback SST should have a decreasing trend. As ISMR is a result of low-level moisture convergence, a higher SST over the IO would be associated with higher moisture availability and should be associated with stronger ISMR. Therefore, the association of a decreasing trend of ISMR and an increasing trend of SST over the IO during this period is counterintuitive. Hence, instead of the increasing trend of SST over the IO during this period driving the decreasing trend of ISMR, it is more likely that the large-scale wind changes associated with the decreasing trend of ISMR is driving the increasing trend of SST. We propose that the change in large-scale vorticity due to the weakening of monsoon circulation during that period played a role in the warming trend. There are two other manifestations of low-level atmospheric circulation, which might have potentially contributed to SST changes over the IO during the P2. Firstly, apart from the equatorial zonal wind, the large-scale low-level monsoon winds over IO, are associated with off-equatorial vorticity, which leads to deepening or shoaling of the thermocline. This mechanism is particularly effective in influencing SST in regions where the mean thermocline is shallow, such as the eastern equatorial IO and the central Indian Ocean thermocline dome, south of the equator. The other factor that could also contribute to the SST changes is the net heat flux (Q_{net}) at the surface as a result of surface wind changes and changes in the cloudiness. In this section, we explore the contributions of large-scale vorticity.

The leading EOFs of vorticity of zonal mean surface zonal winds during the monsoon season for the periods P1 and P2 are shown in Fig. 6a,b while the corresponding PCs for the two periods are shown in Fig. 6c,d. From Fig. 6c and 6d, we see a decreasing trend during P1 and an increasing trend during P2, both statistically significant at 0.05 level from a Mann-Kendall test. The leading EOFs (Fig. 6a,b) indicate important changes in the large-scale monsoon winds over the IO from P1 to P2. While during P1, a cyclonic vortex centered on the equator dominated the wind pattern, during P2, a pair of cyclonic vortices on either side of the equator seems to dominate the low-level wind pattern. This is clearly evident in the vector wind pattern associated with the PC1 of vorticity arising from meridional shear of the zonal mean

surface zonal winds (Fig. 7a,b). A regression of the PC1 of vorticity of zonal mean surface zonal winds on seasonal mean rainfall over India (Fig. 6e,f) indicates that the significantly increasing trend of the PC1 contributes to a strong negative trend of ISMR during the period P2. On the other hand, during the period P1, the decreasing trend of the PC1 is associated with a positive trend of rainfall anomaly pattern over most of India strengthening ISMR more in the early part of the period and less during the latter part of the period resulting in a relatively weak increasing trend of ISMR consistent with Fig. 1a.

Furthermore, a regression of JJAS SST on to the PC1 indicates a positive SST anomaly in the central IO (Fig. 7c) induced by the trend in low level meridional shear of zonal wind (-d[u]/dy) in P1. Similar regression analysis for the P2 indicates a positive SST anomaly in the equatorial eastern IO flanked by colder SST anomaly in the western equatorial IO (Fig. 7d). The larger positive SST anomaly over the central south-equatorial IO is consistent with the cyclonic low-level wind vortex sitting over the thermocline dome in that region. In period P2, large-scale vorticity forcing increases the positive SST anomaly over a much larger region (Fig. 7d) compared to that due to direct zonal wind forcing at the equator (Fig. 4d). The positive SST anomaly over the Bay of Bengal is consistent with the northern component of the twin cyclonic vortices (Fig. 7b). The fact that PC1 during the P2 has a significant increasing trend indicates that the large-scale vorticity of the monsoon flow over the region does contribute to the increasing trend of SST over IO during P2.

Like the SST over the tropical IO, the vertically integrated moisture content in the atmosphere over the Indian monsoon region (70^oE-100^oE, 10^oN-30^oN) is increasing steadily from 1901 to 2007 (Fig. S2a) while the ISMR has an increasing trend during P1 and a decreasing trend during P2. As the ISMR is driven largely by moisture convergence rather than local moisture availability, an increasing trend of vertically integrated moisture convergence during P1 and decreasing trend of the same during P2 are consistent with trends of ISMR during the two periods (Fig. S2b). What makes the moisture convergence decrease during P2 in the backdrop of the moisture content of the atmosphere that has been increasing? The answer lies in the changes of the large-scale winds. The wind changes have led to a decreasing trend of wind convergence (Fig. S2c) that forced the moisture convergence to decrease even when the moisture content was increasing.

3.3 Net heat flux (Q_{net}) driving of SST trend

However, the increasing trend of SST during P2 is much stronger than that during P1 (Fig. 1b) the changes in SST forced by Bjerknes feedback or by the large-scale vorticity of zonal winds appear inadequate to explain the differences in the trends. As we noted, the two different phases of the ISMR MDM P1 and P2 are associated with significant changes in the large-scale circulation, particularly surface winds. These changes in circulation are bound to be associated with changes in cloudiness distribution. As a result, it may be natural to expect that the net heat flux (Q_{net}) would have similar changes during the two periods. The climatological mean Q_{net} during JJAS over the tropical IO between 20S and 20N is positive (~10Wm^{-2}, see Fig. 8) leading to seasonal warming of SST over the region during the summer season. Here we explore if the changes in Q_{net} over the period could also contribute to

an increasing trend of the seasonal warming leading to an overall weaker increasing trend of SST during P1 and a stronger increasing trend during P2.

The net heat flux into the ocean is a sum of different heat exchange processes at ocean surface, which includes heating due to net shortwave radiation (NSWR), net outgoing longwave radiation (NLWR), sensible heat flux (SHF), and latent heat flux (LHF). Climatologically, the first one is the contributor to the heat gain of the ocean, and all the other processes lead to heat loss, except for SHF, which depends on air–sea temperature difference. From all the four variables net heat flux can be calculated using the formula:

Q_{net} = NSWR-NLWR-LHF-SHF (1)

Where, NSWR = DSWR − USWR and NLWR = ULWR – DLWR, together with,

Downward shortwave radiation (DSWR), Upward shortwave radiation (USWR), Upward longwave radiation (ULWR), Downward longwave radiation (DLWR) (e.g., Pokhrel et al. 2020)

A simple thermodynamic understanding about the upper ocean is that the rate of change of SST is proportional to net heat flux. Such a balance can be expressed as

$hC\rho\ (\delta/\delta t\ SST) = Q_{net}$, (2)

where, h is the depth of the mixed layer, C is the specific heat of seawater; ρ is the density of seawater and Q_{net} is net heat flux (e.g., Sengupta et al. 2001). Here mixed layer depth is calculated using the density criteria (Kazunori et al. 2004), i.e., starting from the upper- most available observation to the depth at which the density is equal or greater than a specific value (e.g., 0.125 g/cm^3) than that at the surface is considered as the mixed layer depth (MLD).

To be consistent with SST and precipitation (ISMR), here we use the mean JJAS Q_{net} between 1901 to 2007 to estimate its contribution to the SST trends during the two periods, P1 and P2. However, we recognize that all heat flux products, whether from reanalysis or ‘observations’ have their own biases (Pokhrel et al. 2020). To have an idea of biases in Q_{net} climatology from NCEPv3, we compare the climatology of JJAS Q_{net} from NECPv3 for the two periods (Fig. 8a,b) with those from two other flux products namely from ERA-20CM (Fig. 8c,d) and TROPFlux (Fig. 8e). The TROPFlux data is available only for the period 1979-2018 and hence its climatology may be compared only with P2.

It is interesting to note that the Q_{net} averaged over the tropical IO region, defined as bound by 50°E-100°E, 20°S-20°N, during P1 has a statistically significant decreasing trend (p = 0.001) from about +13 Wm^{-2} to about +5 Wm^{-2} while that during P2 has a weakly significant increasing trend from about +24 Wm^{-2} to about +29 Wm^{-2} (Fig. 9a,b). The net heat flux leads to a statistically significant (p = 0.003) decreasing trend of mixed layer temperature (Fig. 9c) resulting in approximately 0.5^{O}C decrease during P1. It is

interesting to note that the Q_{net} during the P2 drive a statistically significant increasing trend (p = 0.02) of mixed layer depth temperature resulting in an increase of $0.75^{O}C$ during P2 (Fig. 9d).

Discussion

A rather strikingly-decreasing trend of ISMR during the period 1951 to 2000 encouraged several studies to investigate potential drivers for this trend. Ocean-atmosphere interaction involving increasing trend of SST over the IO during that period (Swapna et al. 2014) and a stronger cooling of the land surface compared to the IO by anthropogenic aerosols (Bollasina et al. 2011) have been invoked to explain the trend. However, reconstruction of Indian monsoon rainfall over the past two millennia indicate that such a decreasing trend of ISMR over 50-60 years could as well be part of a multi-decadal variability of the ISMR (Goswami et al. 2015; Sinha et al. 2011). The primary driving of the multi-decadal variability of the ISMR with an approximate period of 65 years appears to be external forcing through its strong association with a similar multi-decadal variability of North Atlantic SST (Goswami et al. 2006; Rajesh and Goswami 2020; Krishnamurthy and Krishnamurthy 2016; Naidu et al. 2020). As local ocean-atmosphere interactions play an important role in maintaining the annual cycle and interannual variability of ISMR and SST over the IO, they may play a role in modifying the multi-decadal variability as well. While the work of Swapna et al. (2014) provide a glimpse of how local ocean-atmosphere feedback could operate on one phase of multi-decadal variability of ISMR, similar ocean-atmosphere interaction in opposite phases of the ISMR multi-decadal variability has been lacking. In addition to the primary Bjerknes feedback between equatorial wind forcing and SST, large-scale vorticity feedback could also influence the SST in the Indian monsoon region with an off-equatorial heat source. The changes in climatological winds and cloudiness due to changes in the monsoon heat source on multi-decadal time scale could influence SST over the IO differently during opposite multi-decadal phases of ISMR through the two local feedbacks. Therefore, it is important to unravel and contrast the ocean-atmosphere feedback at least in two opposite phases of ISMR multi-decadal variability.

The period between 1901 and 2007, with a decreasing phase of ISMR between 1958 and 2007 and an increasing phase during 1901 and 1957, approximately represent two opposite phases of ISMR multi-decadal variability, and provide us an opportunity to examine local ocean-atmosphere interaction during two opposite phases of ISMR. For this purpose, surface winds that are internally consistent with the data sets of monsoon rainfall (ISMR) and SST are essential. The observed ISMR is not necessarily consistent with various independent analyses of surface winds and SST, as observed precipitation is not used to constrain these analyses. Therefore, we need to use a 20^{th} Century reanalysis for our study of air-sea interaction, where the analysis system generated precipitation over the Indian region during the summer monsoon season is consistent with surface winds and the winds are consistent with SST. For our analysis of the air-sea interaction to be meaningful to observed multi-decadal variability of ISMR, however, the analyzed ISMR, from the 20^{th} century reanalysis should have multi-decadal variability similar to that from the observed during the period between 1901 and 2007. We find that the reanalyzed-ISMR in NCEPv3 (Fig. 1c) follows the multi-decadal variability in the observed ISMR (Fig. 1a) during the

period, while the multi-decadal variability from the ERA-20CM (Fig. S3) during the same period has phases that are opposite to those of ISMR. For this reason, winds from NCEPv3 and SST from HadISST, where the SST is consistent with the winds have been used in this study to examine air-sea interaction during two opposing phases of ISMR.

Our results indicate that the basic multi-decadal oscillation of ISMR may be driven by teleconnection with North-Atlantic SST, but a local Bjerknes feedback and a large-scale vorticity help to maintain and modify it. During the increasing phase of ISMR (P1), a higher propensity of occurrence of a positive IOD pattern of SST anomaly with cold water in the eastern Indian IO while warm waters in the western IO reinforce easterly equatorial surface winds that drive them. During a decreasing phase of ISMR (P2), just the opposite happens, with a higher propensity of negative IOD events reinforcing the westerly equatorial surface winds that drive them. The Bjerknes feedback, however, does not contribute significantly to the trend of SST over the IO on multi-decadal time scale. We also note that the SST influences the ISMR and ISMR influences the winds and cloudiness distribution and thereby influences the Q_{net}. Therefore, the JJAS mean Qnet contains some of the other two contributions through ISMR influence. It is also noted that over most part of the IO, SST is driven by the Q_{net} except small regions over the coasts of Somalia and Sumatra where upwelling is important. Thus, the Qnet largely drives the SST over 20^{O}S and 20^{O}N and 70^{O}E and 100^{O}E. While we could comment on their contributions to the SST (or mixed layer trends), therefore, it is not fair to combine them to estimate a combined contribution to the SST trend. With this caveat, we examined the contributions of vorticity feedback and Q_{net} to the stronger increasing trend of SST over IO during P2 and find that it is consistent with additive contributions to increasing trends of SST due to the large-scale vorticity forcing and SST forced by Q_{net} during the period. However, a similar comparison during the period P1 indicates that the small increasing trend of SST in the backdrop of a decreasing trend of Q_{net} could not be explained by the weak increasing trend of contributions from vorticity feedback. The result indicates that some of the missing physics such as advection and entrainment may be important in maintaining the weak increasing trend of SST during P1. The overall weak increasing SST trend during P1 is consistent with the weaker increasing SST trends over most regions and a weak negative trend south of 10^{O}S between 60°E to 80°E (Fig. 3a). It may be noted that the first order influence on the SST trend comes from the climatological JJAS mean Q_{net} (Fig. 8e) with cooling tendency south of 10^{O}S and warming tendency north of it. The negative or weak positive SST trend south of 10^{O}S and positive SST trend north of it during both periods (Fig. 3) are consistent with the spatial structure of climatological $Q_{net.}$ The actual trend of SST at any location will also depend on the mean mixed layer depth with the deepest mixed layer being south of 10^{O}S and shallower mixed layers over the equatorial belt and North Bay of Bengal (Fig. S4b). The largest SST trends (Fig. 3) around the equatorial belt are again consistent with this. The trends of Q_{net} and mixed layer depth (MLD) during the period P1 (Fig. S4 a,c) add second-order trends on the SST. The negative SST south of trend 10^{O}S during P1 is a result of the combined influence of the two forces.

The anomalous changes in the climatological low-level winds during the two periods, P1 and P2 (Fig. 7a,b) are the key to explain the differences in air-sea interaction during the two opposite phases of the ISMR multi-decadal oscillation. Once the background winds for a phase are established (like that during P1), the air-sea interaction sets up SST distribution conducive for strong monsoon and perpetuates the easterlies at the equator until the wind climatology is changed to westerlies to reverse this process. We envisage the transition to take place in the following way. Let us start with the positive AMO phase and increasing trend of ISMR like the period P1. When the NA SST MDM changes to a negative phase, it starts introducing westerly zonal wind forcing over the equator. However, the ISMR is still in the positive MDM phase supporting easterly zonal winds at the equator. Therefore, it takes a few years for the westerly to weaken the ISMR so that it start supporting the westerly forcing at the equator and to establish the opposite feedback. A negative phase of ISMR MDM gets established. As shown by Rajesh and Goswami (2020) there is a phase lag between the ISMR multi-decadal mode (MDM) and the North-Atlantic SST MDM with the latter leading by 8 years. This lag is consistent with the proposed mechanism of transition. And hence, two specific periods of ISMR like P1 and P2 could not be exactly matched with two phases of the AMO.

Declarations

Funding: Not applicable

Conflict of interest/Competing interest: No conflict of interest

Availability of data and material:

(a) The monthly gridded data of sea surface temperature (SST) for the period 1901-2007 has been taken from Hadley Center, UK Met Office. The data can be obtained from:
https://www.metoffice.gov.uk/hadobs/hadisst/data/download.html

(b) Daily gridded rainfall data for the period 1901-2007 has been taken from Indian Meteorological Department (IMD). This data can be obtained from:
https://www.imdpune.gov.in/Clim_Pred_LRF_New/Grided_Data_Download.html

(c) NCEP 20th Century Reanalysis V3 data products for the period 1901-2007: Surface wind, winds at 850hPa, net downward shortwave radiation flux, net upward longwave radiation flux, sensible heat flux, latent heat flux, specific humidity, and gridded rainfall datasets can be obtained from:
https://psl.noaa.gov/data/gridded/data.20thC_ReanV3.html

(d) Simple Ocean Data Assimilation version 2 data products for the period 1901-2007: Surface current, Ocean heat content, sea surface height datasets can be obtained from:

http://apdrc.soest.hawaii.edu/las/v6/dataset?catitem=4866

(e) ERA-20CM data products for the period 1901-2007: Net downward shortwave radiation flux, net upward longwave radiation flux, sensible heat flux, latent heat flux, and gridded rainfall datasets can be obtained from:

https://www.ecmwf.int/en/forecasts/datasets/browse-reanalysis-datasets

(f) Net heat flux dataset for the period 1979-2018 has been taken from INCOIS and can be obtained from: https://incois.gov.in/tropflux/

Code availability: Used MATLAB and climate data operator (CDO)

Acknowledgement

BNG is grateful to the Science and Engineering Research Board (SERB), Government of India for the SERB Distinguished Fellowship and Research grant. Dhruba Jyoti Goswami wants to thank Department of Physics, Cotton University for providing the required facilities and Center for Earth, Ocean and Atmospheric Sciences (CEOAS), University of Hyderabad for the encouragement and support to carry out this research. We are grateful to three anonymous reviewers for constructive comments and suggestions on an earlier version of the manuscript that led to a significant improvement of the manuscript.

References

1. Amat HB, Ashok K (2018) Relevance of Indian Summer Monsoon and its Tropical Indo-Pacific Climate Drivers for the Kharif Crop Production. Pure Appl. Geophys. 175**,** 2307–2322 https://doi.org/10.1007/s00024-017-1758-9
2. Amat HB, Pradhan M, Tejavath CT (2021) Value addition to forecasting: towards Kharif rice crop predictability through local climate variations associated with Indo-Pacific climate drivers. Theor Appl Climatol 144**,** 917–929 https://doi.org/10.1007/s00704-021-03572-6
3. Ashok K, Guan Z, Yamagata T (2001) Impact of the Indian Ocean Dipole on the between the Indian Monsoon Rainfall and ENSO, Geophys. Res. Letts. 28(23), 4449-4502
4. Ashok K, Guan Z, Saji NH and Yamagata T (2004) Individual and Combined Influences of ENSO and the Indian Ocean Dipole on the Indian Summer Monsoon, J. Climate, 17, 3141-3155.
5. Bjerknes J (1969) Atmospheric teleconnections from the equatorial Pacific. Mon. Wea. Rev., 97 **,** 163–172.
6. Blanford HF (1884) On the Connection of the Himalaya Snowfall with Dry Winds and Seasons of Drought in India. Proceedings of the Royal Society of London, 37, 3– 22.doi:10.1098/rspl.1884.0003
7. Bollasina MA, Ming Y, Ramaswamy V (2011) Anthropogenic Aerosols and the Weakening of the South Asian Summer Monsoon, Science, 334, 502-505 DOI: 10.1126/science.1204994
8. Borah PJ, Venugopal V, Sukhatme J, Muddevihal P, Goswami BN (2020) Indian monsoon derailed by a North Atlantic wavetrain, Science 370, 1335–1338, DOI: 10.1126/science.aay6043

9. Burns SJ, Fleitmann D, Matter A, Kramers J and Al-Subbary AA (2003) Indian Ocean climate and an absolute chronology over Dansgaard/Oeschger events 9 to 13. Science, 288, 847– 850.
10. Charney JG & Shukla J (1981) Predictability of monsoons, in Monsoon Dynamics, Lighthill J and Pearce, (Eds), Cambridge University Press, pp. 99–108
11. Choudhury BA, Rajesh PV, Zahan Y and Goswami BN (2021) Evolution of the Indian Summer Monsoon Rainfall Simulations from CMIP3 to CMIP6 Models, Climate Dynamics, https://doi.org/10.1007/s00382-021-06023-0
12. Gadgil S, Gadgil S (2006) The Indian Monsoon, GDP and Agriculture. Economic & Political Weekly, Vol – XLI: No. 47, November 25.
13. Giese BS and Ray S (2011) El Niño variability is simple ocean data assimilation (SODA), 1871-2008, J. Geophys. Res., 116, C02024, doi:10.1029/2010JC006695.
14. Goswami BN, Madhusoodanan MS, Neema CP & Sengupta D (2006a). A physical mechanism for North Atlantic SST influence on the Indian summer monsoon. Geophysical Research Letter, 33, L02706,doi:10.1029/2005GL024803.
15. Goswami BN, Wu G & Yasunari T(2006b) The Annual Cycle, Intra-seasonal Oscillations, and Roadblock to Seasonal Predictability of the Asian Summer Monsoon. Journal of Climate,19, 5078-5099.
16. Goswami BN, Kriplani RH, Borgaonkar HP & Preethi B (2015) Multi-decadal variability of Indian summer monsoon rainfall using proxy data, Climate Change : Multi-decadal and beyond, Chapt. 21, pp. 327-346, (Editors: C.P. Chang, Michael Ghil, Mojib Latif, and Mike Wallace), World Scientific, New Jersey, London, Singapore, Beijing, Chennai
17. Goswami BN, Krishnan R (2013) Opportunities and challenges in monsoon prediction in a changing climate - Editorial of Special OCHAMP issue, Clim. Dyn., vol. 41, July 2013, DOI:10.1007/s00382-013-1835-4, 1
18. Gupta AK, Anderson DM & Overpeck JT (2003) Abrupt changes in the Asian southwest monsoon during the Holocene and their links to the North Atlantic Ocean. Nature, 421, 354–357.
19. Hersbach H, Peubey C, Simmons A, Berrisford P, Poli P and Dee D (2015) ERA-20CM: a twentieth-century atmospheric model ensemble. Q.J.R. Meteorol. Soc, 141: 2350-2375. https://doi.org/10.1002/qj.2528
20. Jin Q, Wang C (2017) Revival of Indian summer monsoon rainfall since 2002. Nature Clim Change **7,** 587–594. https://doi.org/10.1038/nclimate3348
21. Johannes L, Webster PJ (2000) A Coupled Ocean–Atmosphere System of SST Modulation for the Indian Ocean **,***J. Climate* (2000) **13** (19): 3342–3360, https://doi.org/10.1175/1520-0442(2000)013<3342:ACOASO>2.0.CO
22. Kapil S (2021) Agri share in GDP hit 20% after 17 years: Economic Survey, Down to Earth, Friday, 29 January, 2021.
23. Kemball-Cook S & Wang B (2001) Equatorial waves and air-sea interaction in the boreal summer intraseasonal oscillation. Journal of Climate, 14(13), 2923–2942. https://doi.org/10.1175/1520-

0442(2001)014

24. Kripalani RH and Kulkarni A (1997) Climatic impact of El Nin˜o/ La Nin˜a on the Indian monsoon: A new perspective. Weather, 52, 39–46.
25. Krishnamurthy L and Krishnamurthy V (2016) Teleconnections of Indian monsoon rainfall with AMO and Atlantic tripole, Clim Dyn (2016) 46:2269–2285
26. Krishnamurthy V & Goswami BN (2000) Indian Monsoon–ENSO Relationship on Interdecadal Timescale. Journal of Climate, 13, 579-595.
27. Kumar BP, Vialard J, Lengaigne M, Murty VSN, McPhaden MJ (2012a) TropFlux: Air-Sea Fluxes for the Global Tropical Oceans - Description and evaluation, Climate Dynamics, 38, 1521-1543, doi:10.1007/s00382-011-1115-0
28. Kumar KK, Soman MK, Rupa Kumar K (1995) Seasonal forecasting of Indian summer monsoon rainfall: A review. Weather, 449-467, https://doi.org/10.1002/j.1477-8696.1995.tb06071.x
29. Kumar KK, Rajagopalan B, Cane MA (1999) On the Weakening Relationship Between the Indian Monsoon and ENSO. *Science*,Vol. 284, Issue 5423, pp. 2156-2159,DOI: 10.1126/science.284.5423.2156
30. Lau WKM, Waliser DE, Goswami BN (2012) South Asian monsoon. Intraseasonal Variability in the Atmosphere-Ocean Climate System. Springer Praxis Books. Springer, Berlin, Heidelberg. https://doi.org/10.1007/978-3-642-13914-7_2
31. Li S, Perlwitz J, Quan X, & Hoerling MP (2008) Modelling the influence of North Atlantic multi-decadal warmth on the Indian summer rainfall. Geophysical Research Letters, 35, L05804, doi:10.1029/2007GL032901.
32. Lu R, Dong B & Ding H (2006) Impact of the Atlantic Multi-decadal Oscillation on the Asian summer monsoon. Geophysical Research Letters,33,L24701, doi:10.1029/2006GL027655.
33. Luo F, Li S and Furevik T (2011) The connection between the Atlantic Multidecadal Oscillation and the Indian Summer Monsoon in Bergen Climate Model Version 2.0, J. Geophys. Res., 116, D19117, doi:10.1029/2011JD015848
34. Luo F, Li S, Gao Y, Keenlyside N, Svendsen L, Furevik T (2018) The connection between the Atlantic multidecadal oscillation and the Indian summer monsoon in CMIP5 models, Climate Dynamics (2018) 51:3023–3039, https://doi.org/10.1007/s00382-017-4062-6
35. Mantua NJ, Hare SR (2002) The Pacific Decadal Oscillation. Journal of Oceanography 58**,** 35–44 https://doi.org/10.1023/A:1015820616384
36. Marathe SM, Terray P & Ashok K (2021) Tropical Indian Ocean and ENSO relationships in a changed climate. Clim Dyn 56**,** 3255–3276 https://doi.org/10.1007/s00382-021-05641-y
37. Meehl GA & Arblaster JM (2002) The Tropospheric Biennial Oscillation and Asian–Australian Monsoon Rainfall, J. Climate, 15, 722-744.
38. Meehl GA (1994) Coupled Land-Ocean-Atmosphere Processes and South Asian Monsoon Variability. Science, 266 (5183), 263-267.

39. Mishra V, Smoliak BV, Lettenmaier DP, Wallace JM (2012). A prominent pattern of year-to-year variability in Indian Summer Monsoon Rainfall. Proceedings of the National Academy of Sciences, 109(19): 7213–7217. https://doi.org/10.1073/pnas.1119150109.
40. Murtugudde R, McCreary JP and Busalacchi AJ (2000) Oceanic processes associated with anomalous events in the Indian Ocean with relevance to 1997–1998, J. Geophys. Res., 105(C2), 3295– 3306, doi:10.1029/1999JC900294.
41. Naidu PD, Ganeshram R, Bollasina MA, Panmei C, Nürnberg D & Donges JF (2020) Coherent response of the Indian Monsoon Rainfall to Atlantic Multi-decadal Variability over the last 2000 years, Scientific Reports, https://doi.org/10.1038/s41598-020-58265-3
42. Palmer TN (1994) Chaos and Predictability in Forecasting the monsoon, Proc. Indian Natl. Sci. Aca., 60A, 57-66.
43. Parthasarathy B, Munot AA and Kothawale DR (1988) Regression Model for Estimation of Indian Foodgrain Production from Summer Monsoon Rainfall, Agricultural and Forest Meteorology, 42 (1988) 167-182
44. Pokhrel S, Dutta U, Rahaman H, Chaudhari H, Hazra A, Saha SK & Veeranjaneyulu C (2020). Evaluation of different heat flux products over the tropical Indian Ocean. Earth and Space Science, 7, e2019EA000988. https://doi. org/10.1029/2019EA000988
45. Rajeevan M, Bhate J, Kale JD, Lal B (2006) A high resolution daily gridded rainfall data for the Indian Region: analysis of break and active monsoon spells. Curr Sci 91:296–306
46. Rajesh PV and Goswami BN (2020) 'Four-dimensional Structure and Sub-Seasonal Regulation of the Indian summer Monsoon Multi-Decadal Mode'. Climate Dynamics, DOI 10.1007/s00382-020-05407-y
47. Rao SA, Goswami BN, Sahai AK, Rajagopal EN, Mukhopadhyay P, Rajeevan M et al. (2019) Monsoon mission: A targeted activity to improve monsoon prediction across scales. Bulletin of American Meteorological Society, 100, 2509–2532. https://doi.org/10.1175/BAMS-D-17-0330.1
48. Roxy MK, Ritika K, Terray P, and Masson S, 2014 The Curious Case of Indian Ocean Warming, https://doi.org/10.1175/JCLI-D-14-00471.1, Page(s): 8501–8509
49. Rayner NA, Parker DE, Horton EB, Folland CK, Alexander LV, Rowell DP, Kent EC and Kaplan A (2003) Global analysis of sea surface temperature, sea ice, and night marine air temperature since the late nineteenth century. J. Geophysics. Res. (Atmospheres), 108(14), 2-1
50. Saha SK, Hazra A, Pokhrel S, Chaudhari HS, Sujith K, Rai A et. al. (2019) Unraveling the mystery of Indian summer monsoon prediction: Improved estimate of predictability limit. Journalof Geophysical Research: Atmospheres, 124, 1-13, https://doi.org/10.1029/2018JD030082
51. Saji NH, Goswami BN, Vinayachandran PN & Yamagata T (1999) A dipole mode in the tropical Indian Ocean. Nature, 401, 360–363.
52. Sengupta D and Ravichandran M (2001) Oscillations of Bay of Bengal sea surface temperature during the 1998 summer monsoon, Geophys. Res. Letts., VOL. 28, NO. 10, 2033-2036.
53. Shukla J (1987) Inter-annual Variability of monsoon, in Monsoons J.S. Fein and P. L. Stephens (Eds), John Wiley and Sons Inc.

54. Sinha A, Berkelhammer M, Mudelsee M et al (2011) The leading mode of Indian Summer Monsoon precipitation variability during the last millennium. Geophys Res Lett 38:L15703. https ://doi.org/10.1029/2011g l0477 13
55. Sinha A, Kathayat G, Cheng H et al (2015) Trends and oscillations in the Indian summer monsoon rainfall over the last two millennia. Nat Commun. https ://doi.org/10.1038/ncomm s7309
56. Slivinski LC, Compo GP, Whitaker JS et al. (2019) Towards a more reliable historical reanalysis: Improvements for version 3 of the twentieth century reanalysis system. Q J R Meteorol Soc 145:2876–2908. https://doi.org/10.1002/qj.3598
57. Sontakke NA, Singh N & Singh HN (2008). Instrumental period rainfall series of the Indian region (1813-2005): revised reconstruction, update and analysis. The Holocene, 18 (7),1055- 1066.
58. Suga T, Motoki K, Aoki Y, Macdonald AM (2004) The North Pacific Climatology of Winter Mixed Layer and Mode Waters. J. Phy. Ocean. .DOI:https://doi.org/10.1175/1520-0485(2004)034<0003:TNPCOW>2.0.CO;2
59. Sun, C., Kucharski, F., Li, J. *et al.* Western tropical Pacific multidecadal variability forced by the Atlantic multidecadal oscillation. *Nat Commun* **8,** 15998 (2017). https://doi.org/10.1038/ncomms15998
60. Sun, C., Li, J., Kucharski, F., Kang, I.-S., Jin, F.-F., Wang, K., et al. (2019). Recent acceleration of Arabian Sea warming induced by the Atlantic-western Pacific trans-basin multidecadal variability. Geophysical Research Letters, 46, 1662–1671. https://doi.org/10.1029/2018GL081175
61. Sun, C., Jianping Li, Fred Kucharski, Jiaqing Xue, and Xiang Li (2018) Contrasting spatial structures of Atlantic Multidecadal Oscillation between observations and slab ocean model simulations. Climate Dynamics, https://doi.org/10.1007/s00382-018-4201-8
62. Swapna P, Krishnan R & Wallace JM (2014) Indian Ocean and monsoon coupled interactions in a warming environment. Clim Dyn **42,** 2439–2454. https://doi.org/10.1007/s00382-013-1787-8
63. Syed FS, Yoo JH, Ko¨rnich H and Kucharski F (2012) Extratropical influences on the inter-annual variability of South-Asian monsoon, Clim Dyn (2012) 38:1661–1674
64. DOI 10.1007/s00382-011-1059-4
65. Webster PJ, Magana VO, Palmer TN, Shukla J, Tomas RA, Yanai M & Yasunari T(1998) Monsoons: Processes, predictability, and the prospectsfor prediction.Journal of Geophysical Research,103 (C7), 14,451-14,518.
66. Webster PJ, Moore AM, Loschnigg JP & Leben RR (1999) Coupled ocean-atmosphere dynamics in the Indian Ocean during 1997-98, Nature, 401, 356-359
67. Walker GT (1924) Correlation in seasonal variations of weather, IV, A further study of world weather. Mem. Indian Meteorological Department, 24, 275-332, 1924.
68. Wang B, Ding Q, Fu X, Kang IS, Jin K, Shukla J, Doblas-Reyes F (2005) Fundamental challenge in simulation and prediction of summer monsoon rainfall. Geophysical Research Letter, 32, L15711, doi: 10.1029/2005GL022734 12.

69. Wang Y, Li S and Luo D (2009) Seasonal response of Asian monsoonal climate to the Atlantic Multidecadal Oscillation, J. Geophys. Res., 114, D02112, doi:10.1029/2008JD010929.
70. Wyrtki K (1973) An equatorial jet in the Indian Ocean, Science, 181, 262-264, DOI: 10.1126/science.181.4096.262
71. Xavier PK, Marzin C and Goswami BN (2007) An objective definition of the Indian summer monsoon season and a new perspective on the ENSO–monsoon relationship, Q. J. R. Meteorol. Soc. 133: 749–764 (2007)
72. Zhang R & Delworth TL (2006) Impact of Atlantic multi-decadal oscillations on India/Sahel rainfall and Atlantic hurricanes. Geophysical Research Letters,33, L17712, doi:10.1029/2006GL026267.
73. Zhang Y, Wallace JM and Battisti DS (1997) ENSO-like Interdecadal Variability: 1900–93, 10, 1004-1020.

Figures

Figure 1

(a) Indian summer monsoon rainfall (ISMR) using Rajeevan et al. (2006) rainfall data normalized by its own interannual standard deviation from 1901 to 2007. The linear trends for the periods 1901 to 1957 (P1) and 1958 to 2007 (P2) are shown. (b) Sea surface temperature averaged over (50°E-100°E, 20°S-20°N) during June-September for the period 1901 to 2007 normalized by its own standard deviation. (c) Normalized ISMR similar to (a) but from NCEPv3.

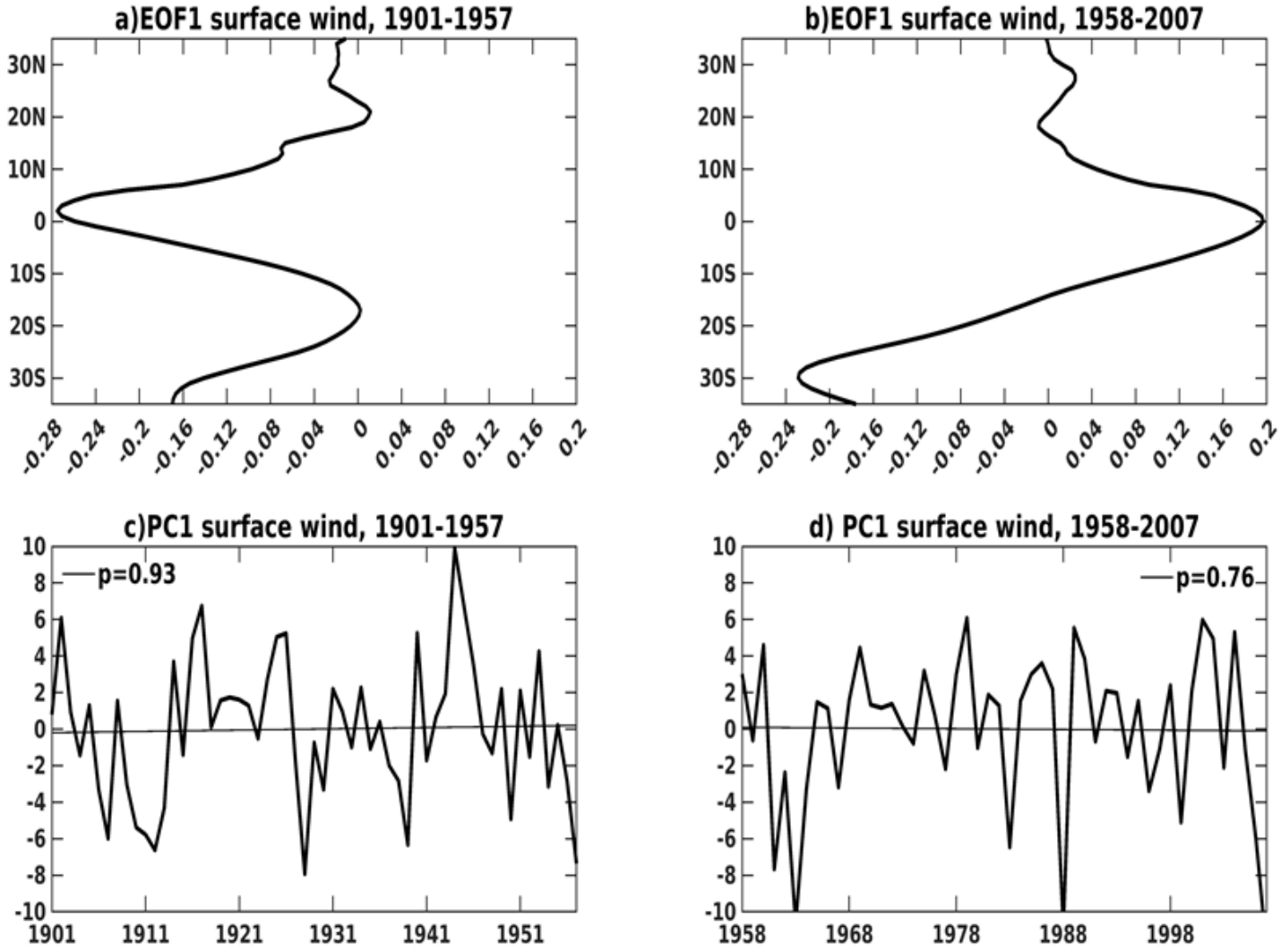

Figure 2

(a) Latitude dependence of the dominant EOF (EOF1) of zonal wind zonally averaged between 70°E and 90°E for the period P1, (b) Same as (a) but for the period P2, (c) Time series of Principal component (PC1) corresponding to EOF1 for the period P1, (d) Same as (c) but for the period P2. The linear trends of the PCs shown by straight lines are statistically insignificant (see p-values).

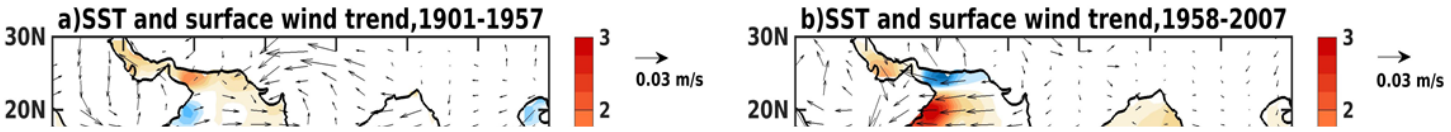

Figure 3

(a) Trends in sea surface temperature (SST in °C/57- years) and NCEPv3 surface winds (m s^{-1} / 57-years) in the tropical Indian Ocean (IO) for the summer monsoon season for period P1. (b) Same as (a) but for period P2. (SST values at grid points are multiplied by 100 for better representation of the colour bar)

Figure 4

(a) Regressed anomaly pattern of seasonal mean rainfall with PC1 of surface zonal wind averaged between 70°E and 90°E during P1. (IMD rainfall data and wind from NCEP v3), (b) Same as (a) but during P2. (IMD rainfall data and wind from NCEPv3) Units: (mm day^{-1})(ms^{-1})$^{-1}$. (c) Regressed anomaly pattern of seasonal mean SST with PC1 of surface zonal wind averaged between 70°E and 90°E during P1. (d) Same as (c) but during P2. Units (°C)(ms^{-1})$^{-1}$.

Figure 5

(a) Surface currents associated with zonal mean zonal wind variability (regression with PC1) during P1 (vectors) together with associated upper ocean heat content (HC) (color), (b) Same as (a) but for P2. Units: HC, (Jm^{-2})(ms^{-1})$^{-1}$, currents, (ms^{-1})(ms^{-1})$^{-1}$, (c) Same as (a) but for sea surface height (SSH) for P1 and (d) same as (c) but for P2. Units: m(ms^{-1})$^{-1}$.

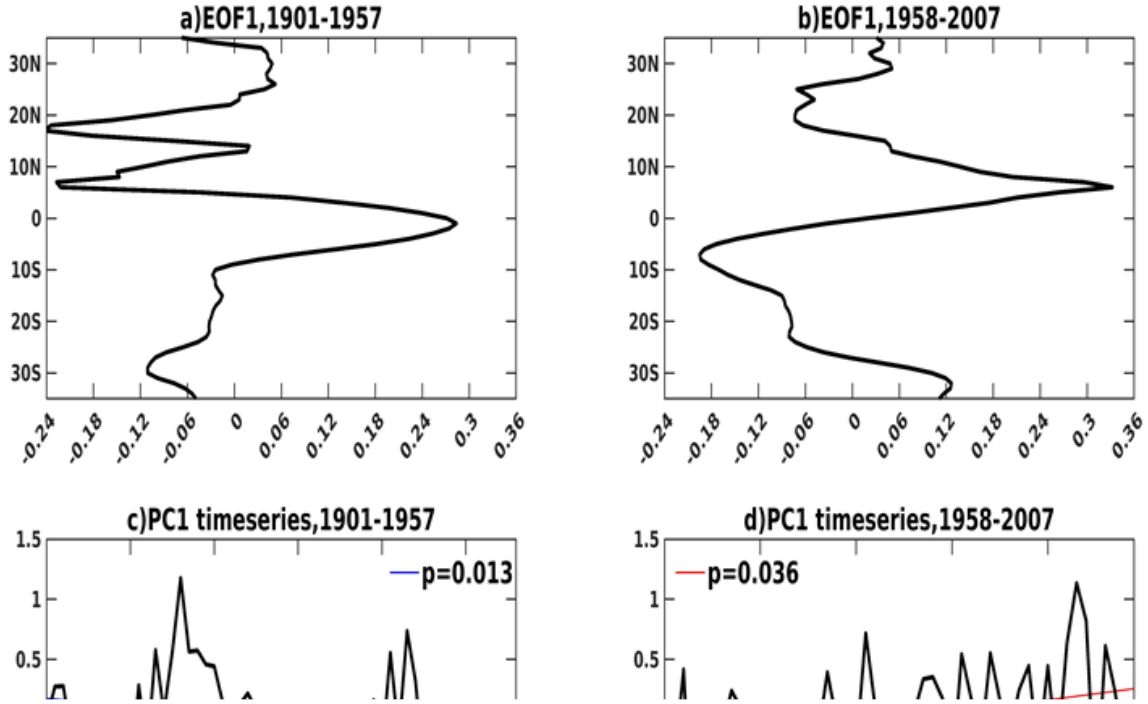

Figure 6

(a) The meridional profile of the leading EOF of (-d[u]/dy) from NCEP-v3 averaged from 70°E to 90°E along a section extending from 35°S to 35°N for the summer monsoon season over the periods (a) 1901-1957 and (b)1958-2007. The time series of the corresponding PC1 for both periods (c) 1901-1957 and (d) 1958-2007. The pattern of rainfall anomalies was obtained by regressing rainfall upon PC1 of (-d[u]/dy) for the summer monsoon season for the periods (e) 1901-1957 and (f) 1958-2007. Unit: (mm day^{-1})(s)

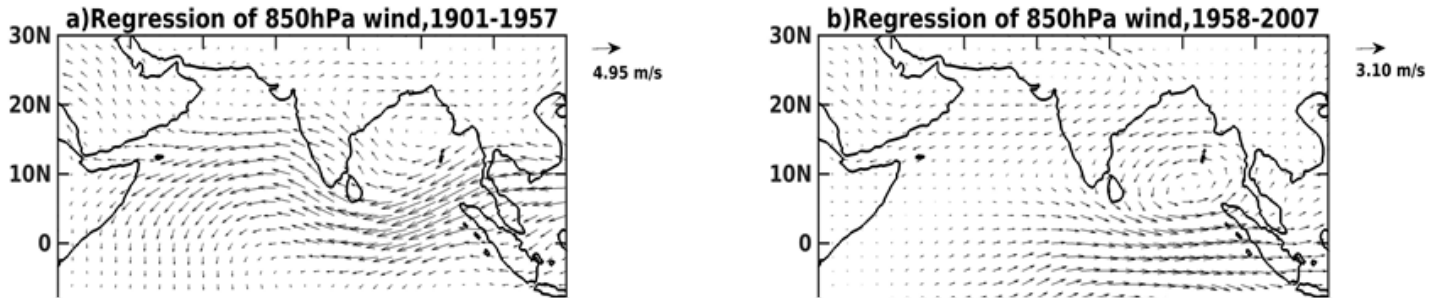

Figure 7

Patterns of 850 hPa winds obtained by regressing wind upon PC1 of (-d[u]/dy) for the summer monsoon season during the periods, (a) 1901-1957 and (b) 1958-2007. Unit:(ms^{-1})(s), Patterns of SST anomalies obtained by regressing SST upon PC1 of (-d[u]/dy) for the summer monsoon season for the periods (c) 1901-1957 and (d) 1958-2007. Unit:(°C)(s)

Figure 8

Comparison of JJAS climatology of Q_{net} from three flux products. (a) From NCEPv.3 for P1, (b) From NCEPv.3 for P2, (c) From ERA-20CM for P1, (d) From ERA-20CM for P2 and (e) From TROPFlux for 1979-2018. (Wm^{-2})

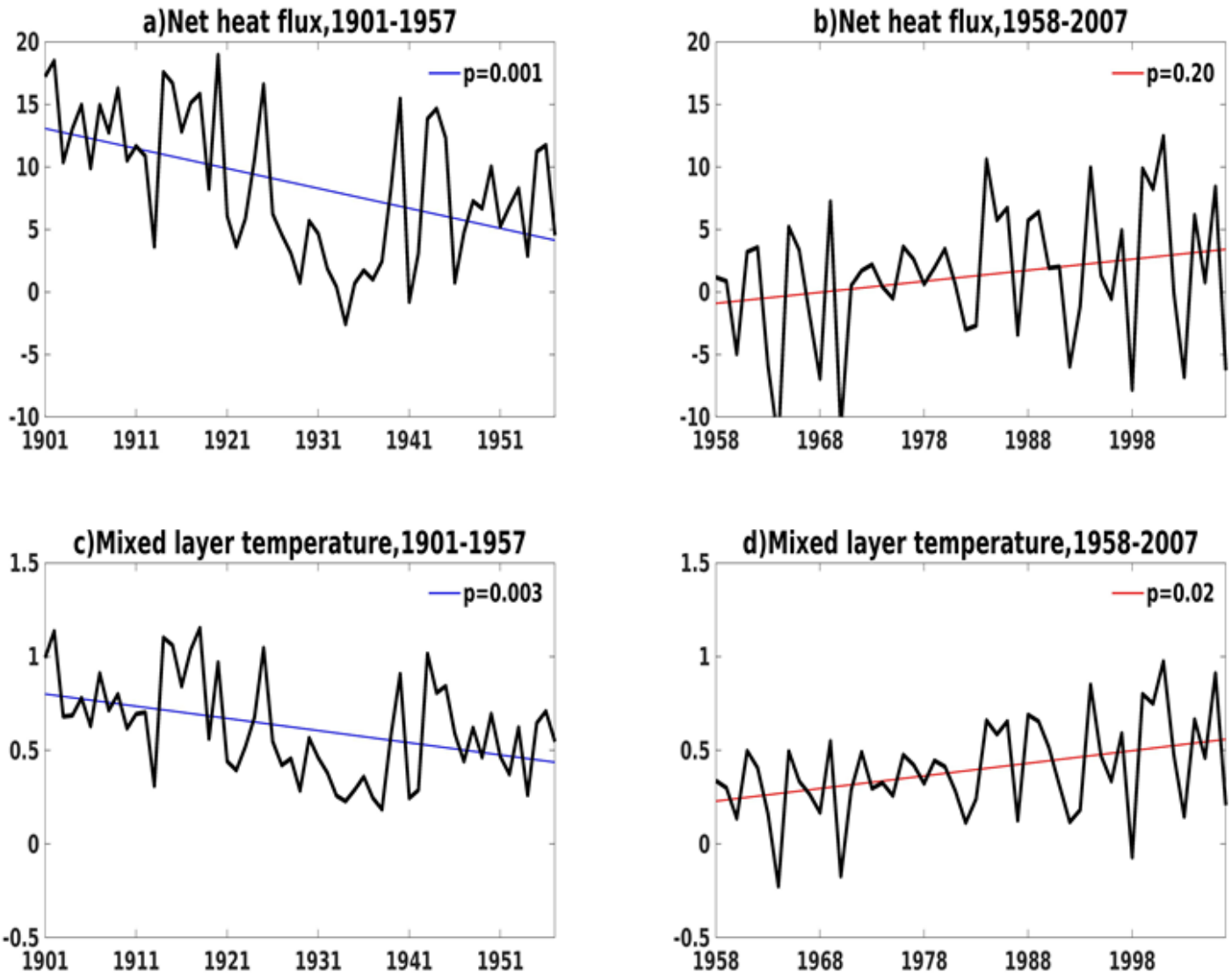

Figure 9

(a) Time series of JJAS mean Q_{net} from NCEPv.3 averaged over (50°E-100°E, 20°S-20°N) for P1 together with its linear decreasing trend (blue line). (b) Same as (a) but for P2. Unit:($W.m^{-2}$). The linear increasing trend is shown by the red line. (c) Time series of mixed layer temperature during the JJAS season forced by Q_{net} during P1. The decreasing linear trend is shown by the blue line. (d) Same as (c) but during P2. The increasing linear trend is shown by the red line. Unit: ($°C.\ day^{-1}$). The p-values for statistical significance of the linear trends are shown.

Supplementary Files

This is a list of supplementary files associated with this preprint. Click to download.

- SupplemantaryMaterial.pdf